Reuse of waste glass addition with industrial wastes and tungsten as new radiation shields: Spectroscopic and computational analysis

Z. Aygun[a,*] and M. Aygun[b]

[a]*Bitlis Eren University, Vocational School of Technical Sciences, 13100, Bitlis,*
[b]*Bitlis Eren University, Faculty of Science and Arts, Department of Physics, 13100, Bitlis, Turkey,*
[*]*e-mail: zeynep.yarbasi@gmail.com*

Received 28 February 2024; accepted 8 May 2026

The economic and environmental problems regarding waste encourage the researchers to reuse the waste and produce new materials. Waste glass, as a form of industrial waste, has gained growing attention in recent years. The objective of conducting this study is to evaluate the waste glasses obtained from our daily routines and to ascertain the radiation shielding capabilities of the waste materials obtained by adding other industrial wastes. With this purpose, three samples including both waste glass and industrial wastes (Bayburt stone dust and Oltu stone dust) were produced by mixing in different ratios. Also, tungsten was added to the samples in order to improve the protection ability. The Phy-X/PSD code was used to determine the radiation protection parameters. In addition to the shielding investigation, structural properties were characterized using EPR, XRD, and SEM-EDS spectroscopic techniques. It is obtained that the shielding performance of the sample including Bayburt stone dust and marble waste with tungsten addition is the highest. The lowest shielding performance is observed for the sample including Oltu stone dust and marble dust with tungsten addition. Neutron shielding capabilities are also found to be the same as photon shielding. It can be concluded that the newly prepared samples consisting of waste glass in order to support reusing and recycling have good protective features and the usage of the samples can be recommended.

Keywords: Waste glass; industrial waste; Phy-X/PSD; radiation shielding capability.

DOI: https://doi.org/10.31349/RevMexFis.72.051201

1. Introduction

Waste glass (WG) is a kind of industrial waste that has become a bigger problem with the increasing population all over the world due to the increase in consumption. Increasing technologies for recycling and reusing waste has become important to focus on. Despite the use of recycling technologies, a large amount of waste glass is still waiting to be evaluated. It can be advantageous to use the waste glass as an alternative to concrete with the properties of being abundant, economical, optically transparent and non-toxic. Soda-lime-silica (SLS) glass is an alternative SiO2 source generally seen in glass containers or window glass such as bottles and jars. Glass can be evaluated as radiation shield material due to its ease of manufacturing, low cost, physical and chemical properties. Radiation protection efficiencies can be changed and developed by addition of different materials. Industrial waste materials such as Bayburt stone dust, marble dust and Oltu stone dust with good refractory properties containing high amounts of silica and calcium, can be also reused to save the environment and contribute to the economy as building materials. Also, waste samples are supported by adding heavy elements such as tungsten (W) to improve shielding ability against harms of radiation [1–3]. W has non-toxicity property, and special features such as a high melting point, low neutron activation, high thermal conductivity, etc. among the high-Z elements.

Oltu stone (OS) with the other names as Black Amber, Erzurum stone or Carbon black, found in Oltu (Erzurum) in Turkey, has a matte and black appearance, after being polished it gains an attractive black shine [4, 5]. Oltu stone is a dense mineral-like substance that resembles coal, but in appearance it is similar to obsidian [6]. Its most striking feature is that it is very soft when carved and maintains its softness even if it is not cut. It hardens when it comes into contact with air. Oltu stone is involved in Erzurum's economy with various aspects such as mining, stone processing, handicraft workshops, sales and trade. Oltu stone waste (OSW) is obtained either from mines or workshops after processing the stone [4]. Marble waste (MW) is generated when cutting marble to produce regular geometric shapes. Due to the growth in the construction industry, the use of marble has increased and therefore MW has increased. MW consisting of dust, stones of irregular shapes and sizes thrown into open fields and roadsides causes environmental and health problems [7]. Bayburt stone (BS) is a natural stone named after the Bayburt province in Turkey. BS have potential use due to their high pozzolanic activity and are ground into powder to be used as a material to replace the binder [8]. Bayburt stone waste (BSW) is formed during the cutting processing of stones in quarries. These wastes are very cheap, easy to find, economical, effective and suitable for different applications.

Radiation, whose benefits cannot be ignored in many fields such as industry, science, agriculture, energy, radiology and medicine, causes serious health problems in the long and short term due to exposure to radiation in everyone working or receiving services in these sectors. Consequently, in recent years, researchers have focused on the development of protective materials with higher radiation absorption abilities by different material types such as composites, glasses, alloys, rocks, polymers, concretes etc. which are novel, non-toxic, cost-effective [1, 9–15]. In addition to these studies, waste materials were also studied widely [7, 10, 14, 16, 17]. The common features make the produced materials attractive are being effective for protection, being eco-friendly, and being designed to minimize environmental pollution.

The target of the study is to produce materials with good attenuation potentials based on waste glass and industrial wastes obtained from some industries. In this context, the shielding parameters; exposure and energy absorption buildup factors (EBF and EABF), mass attenuation coefficients (MAC), linear attenuation coefficients (LAC), effective atomic number (Zeff), half-value layer (HVL), mean free path (MFP), fast neutron removal cross-section (FNRCS) of the samples, have been calculated by the code Phy-X/PSD [18] in this work.

The structural properties were also provided by spectroscopic methods as well as the shielding performances. Electron paramagnetic resonance (EPR) is used for the magnetic features of the systems in the external magnetic field by the microwave frequency. The identification of crystalline phases or amorphous structure of the samples is made by X-ray diffraction (XRD). Scanning electron microscopy (SEM) is used for surface structure and energy dispersive spectroscopy (EDS) is for obtaining the compositional content. The study will show that the wastes and industrial materials can be evaluated in different ways than their current usage areas.

2. Materials and methods

2.1. Sample preparation

Three samples were prepared and named as W1, W2, W3 including waste glass (WG), Oltu stone waste (OSW), Bayburt stone waste (BSW), Marble waste (MW) with addition of tungsten (W). The ratios of the ingredients of the prepared samples are given in Table I. Firstly, glass waste and other wastes were powdered, prepared in certain quantities and placed in porcelain crucibles. Secondly, the mixed materials were melted in the oven at 1100°C for 2 hours. The process continued in the oven at 500°C for 3 hours. Finally, the oven was turned off and the glass samples were allowed to cool until the temperature dropped to room temperature. The obtained glass samples were crushed and made ready for spectroscopic experiments.

2.2. Experimental techniques

Room temperature EPR spectra of the samples were taken by X-band JEOL JESFA300 EPR spectrometer with ≈ 9.2 GHz frequency and 100 kHz (0.0002-2mT) magnetic field modulation amplitude. Samples with 4 mm sizes were prepared and put in diamagnetic tubes for EPR experiment. XRD patterns were taken by BRUKER D8 ADVANCE XRD. X-ray diffractograms of the samples were recorded with a 2.5°/min (40 kV and 40 mA) scanning speed in the range of $2\Theta \approx 10^\circ - 90^\circ$ by Cu-Kα ($\lambda = 1.54060$ Å). SEM images were recorded by ZEISS EVO LS10. EDS results were taken by JEOL JSM-6610 spectrometer.

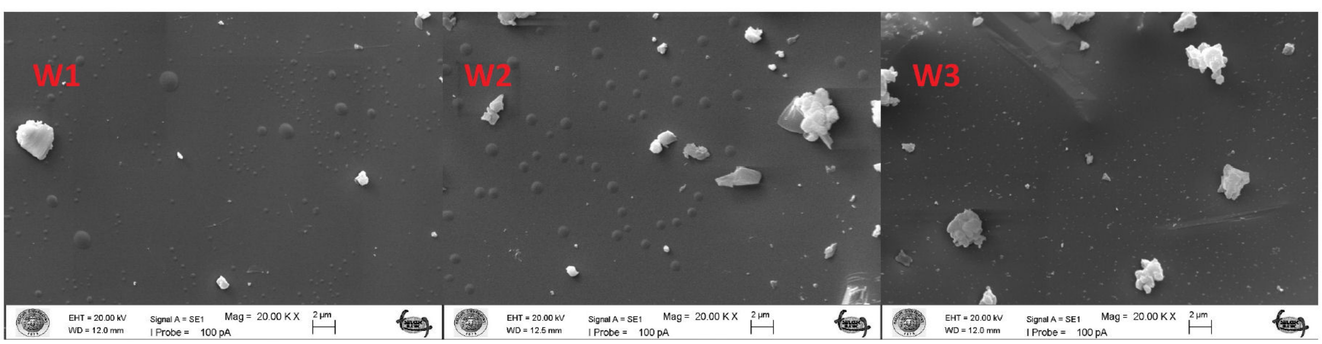

FIGURE 1. SEM images of the samples.

TABLE I. Compositional rate and ingredients of the prepared samples.

W1	Waste Glass (%)	Oltu Stone Waste (%)	Bayburt Stone Waste (%)	W (Tungsten) (%)
	90	2.5	5	2.5
W2	Waste Glass (%)	Oltu Stone Waste (%)	Marble Waste (%)	W (Tungsten) (%)
	90	2.5	5	2.5
W3	Waste Glass (%)	Bayburt Stone Waste (%)	Marble Waste (%)	W (Tungsten) (%)
	90	2.5	5	2.5

TABLE II. Knowledge of the parameters used in the study.

Parameter	Definition	Formula	Unit	Description
ρ_{mix}	The mass per unit volume	$\frac{\sum_{i=1}^{n} c_i A_i}{\sum_{i=1}^{n} (c_i A_i/\rho_i)}$	g/cm^3	c_i: atomic fraction A_i: atomic weight ρ_i: density of element ith [19]
$MAC(\mu_m)$	The attenuation of the radiation per unit mass	$\frac{\mu}{\rho} = \frac{\ln(\frac{I_0}{I})}{t_m}$ or $\frac{\mu}{\rho} = \sum_i w_i (\frac{\mu}{\rho})_i$	cm^2/g	I$_0$ and I: incident and attenuated photon intensities ρ(g/cm^3): density of material t_m(g/cm^2): mass per unit area t (cm): thickness w_i: weight fraction $(\mu/\rho)_i$: mass attenuation coefficient of the ith constituent element [20]
$LAC(\mu)$	The fraction of attenuated incident radiation per unit thickness of a material	$\rho\mu_m$	μ(cm^{-1})	μ_m: the mass attenuation coefficient ρ(g/cm^3): density of material
HVL	The thickness of a shield that half the incident radiation	$\frac{\ln(2)}{\mu}$		μ: the linear attenuation coefficient
MFP	The average distance over which a photon travels before substantially changing its direction or energy	$\frac{1}{\mu}$		μ: the linear attenuation coefficient
$ACS(\sigma_a)$	Interaction probability per atom in a unit volume of any material	$\frac{N}{N_A} (\frac{\mu}{\rho})$	cm^2/g	N_A: Avogadro's number N: atomic mass of materials
$ECS(\sigma_e)$	Interaction probability per electron in a unit volume of any material	$\frac{\sigma_a}{Z_{\text{eff}}}$	cm^2/g	σ_a: the atomic cross section Z_{eff}: the effective atomic number
Z_{eff}	Average atomic number of the compound including more than one element	$\frac{\sigma_a}{\sigma_e}$		Z_{eff}: the effective atomic number σ_a: the atomic cross section σ_e: the electronic cross section
FNRCS ($\sum R$)	The probability of a fast neutron undergoing the first collision that that will remove it from the environment penetrating group of uncollided neutrons	$\sum_i \rho_i (\frac{\sum R}{\rho})_i$	cm^{-1}	$(\frac{\sum R}{\rho})_i$: mass removal cross-section of the ith constituent element ρ_i: the partial density of the material [18]
Z_{eq}	$\frac{Z_1(\log R_2 - \log R) + Z_2(\log R - \log R_1)}{\log R_2 - \log R_1}$			R : $(\mu\text{m})_{\text{Compton}}/(\mu\text{m})_{\text{total}}$ for the material at a specific energy R1, R2: values indicate $(\mu\text{m})_{\text{Compton}}/(\mu\text{m})_{\text{total}}$ ratios of two adjacent elements, with Z_1 and Z_2 atomic numbers

G-P fitting parameters	$\frac{F_1(\log Z_2 - \log Z_{eq}) + F_2(\log Z_{eq} - \log Z_1)}{\log Z_2 - \log Z_1}$	F1, F2: values of G-P fitting parameters identical with the Z_1 and Z_2 atomic numbers at a certain energy [21]
EBF and EABF	$B(E,x) = 1 + \frac{(b-1)(K^x-1)}{(K-1)}$ for $K \neq 1$ $B(E,x) = 1 + (b-1)x$ for $K = 1$ $K(E,x) = cx^a + d\frac{\tanh(\frac{x}{X_k}-2) - \tanh(-2)}{1-\tanh(-2)}$ for $x \leq 40mfp$	E: primary photon energy x: penetration depth a, b, c, d, X_K coefficients of the material [22,23]

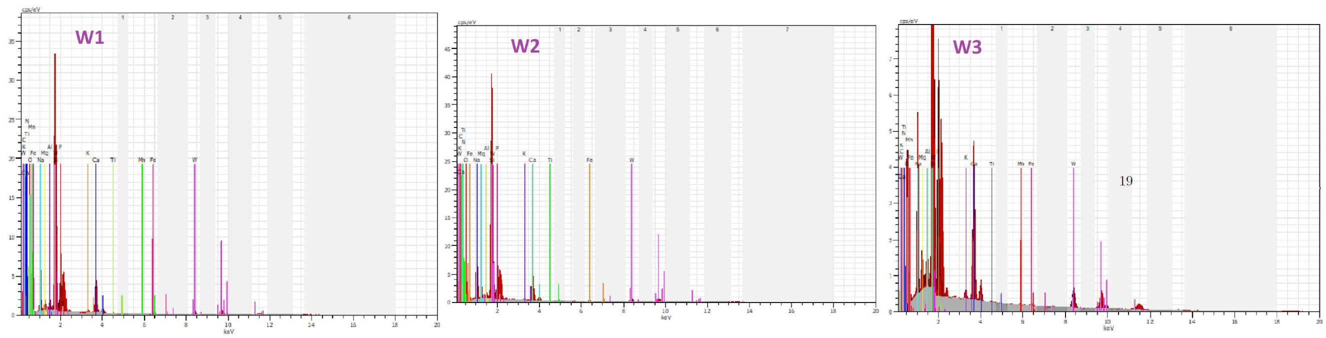

FIGURE 2. EDS results of the samples.

TABLE III.

Samples	O	C	Ca	K	Si	Na	Fe	Ti	Mg	P	Al	Mn	N	W	Density (g/cm^3)
W1	28.07	1.56	9.44	0.52	24.32	7.47	0.37	0.15	1.48	11.16	1.28	0.20	0.03	13.94	3.05
W2	32.82	1.21	7.97	0.45	23.08	10.20	0.33	0.08	2.02	9.06	1.48	-	0.02	11.28	2.73
W3	30.55	1.66	9.89	0.51	22.31	7.11	0.32	0.10	1.33	10.47	1.16	0.13	0.02	14.64	3.10

2.3. Theoretical process

For calculating the parameters by Phy-X/PSD code the composition of the material is entered in two ways such as mole fraction and weight fraction. The knowledge of density (g/cm^3) of the material is also necessary for obtaining the attenuation parameters. The acquired results are supplied in a `MS Excel`. The information about the parameters investigated in the study is given in Table II.

3. Results and discussion

3.1. SEM and EDS analysis

SEM images and EDS spectra of the samples are given in Figs. 1-2. If the micrographs obtained from the surfaces of the samples are studied, smooth surfaces with some micro-crystallites are seen. The weight % ratios of the elements obtained from these spectra are given in Table III. It is understood from the SEM images given in Fig. 1 that all the samples have smooth structures. Air bubbles are observed which were also stated before by Aygun [24]. EDS analysis results were found to be consistent except for W amount. The melting temperature of W is higher than those of the others, so the EDS results give acceptable values different from the casting rates due to the problems that may arise from the incomplete dissolution of the samples for the element of W.

3.2. XRD analysis

XRD patterns recorded at room temperature are given in Fig. 3. The diffraction peaks were examined by the literature [1, 25, 26]. X-ray analysis of the samples shows similar results and the existence of calcite and SiO2 phase peaks. The samples produced by W addition give α-W main phase. It is observed that the samples show more amorphous structure with some crystalline features in XRD patterns.

The crystallite size is calculated by the diffraction pattern depending on the full width half height (FWHM) and the Debye-Scherrer equation [27]. β the FWHM in radians; K the Scherrer's constant and in the order of $\cong$ 0.9; λ the X-ray wavelength, d the average size of the crystalline, and θ the Bragg angle in degrees [1]:

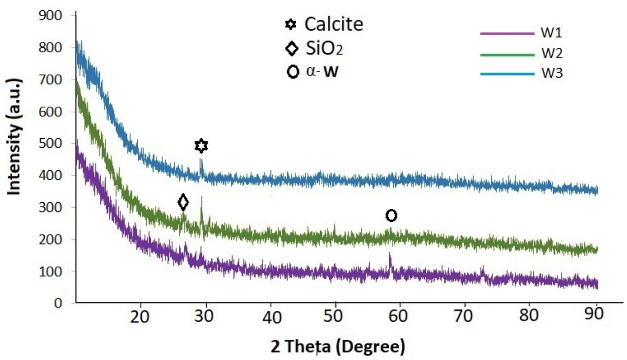

FIGURE 3. XRD patterns of the samples.

$$d = \frac{K\lambda}{\beta \cos\theta}. \quad (1)$$

The presence of the α-W main phase at $\approx$58° has the crystallite size as 50.75 nm. The crystallite size of other main phase at $\approx$29° assigned to calcite is $\approx$68 nm.

3.3. EPR study

EPR is a useful magnetic resonance technique which causes determination of the local chemical environment of magnetically active nuclei (I $\neq$ 0), radicals or paramagnetic centers that have one or more unpaired electrons in their structure. The EPR effect is defined by the observation of transitions in the spin of electrons between energy states in the presence of an external magnetic field; these transitions are known as 'degenerate' when the magnetic field is absent [28, 29]. EPR is based on the measurement of the absorption of electromagnetic radiation in the microwave frequency region by a paramagnetic sample positioned within a magnetic field. It is important to note that these absorptions are observed at specific frequencies and magnetic field combinations, which are known to vary according to the type of paramagnetic species present and its characteristics. Consequently, the lines produced at distinct regions of the scanned magnetic field will vary significantly depending on the type of radical or metal ion under investigation [30]. The EPR lines are identified by g-values and the equation $h\nu = g\beta H$ with β the Bohr magneton, H the magnetic field, h the Planck constant, and ν the microwave frequency is used for the determination of the values. The paramagnetic center by the effect of local magnetic fields on unpaired electrons can be characterized by the g-factor. Therefore, the nature of the EPR signal can be ascribed to a paramagnetic center. EPR spectra of the samples taken at room temperature are given in Fig. 4. Fe^{+3} ions or high-spin isolated Fe^{+3} center is observed with g value of $\approx$4.21 for the samples [28]. A broad EPR signal with g-value of $\approx$ 1.98 which can be ascribed to Mn^{+2} (I=5/2) is detected. In general, it is expected to observe six hyperfine lines of Mn^{+2} but as a result of the random and close localization of Mn ions and their dipole-dipole or exchange interaction a broad signal can be seen [31].

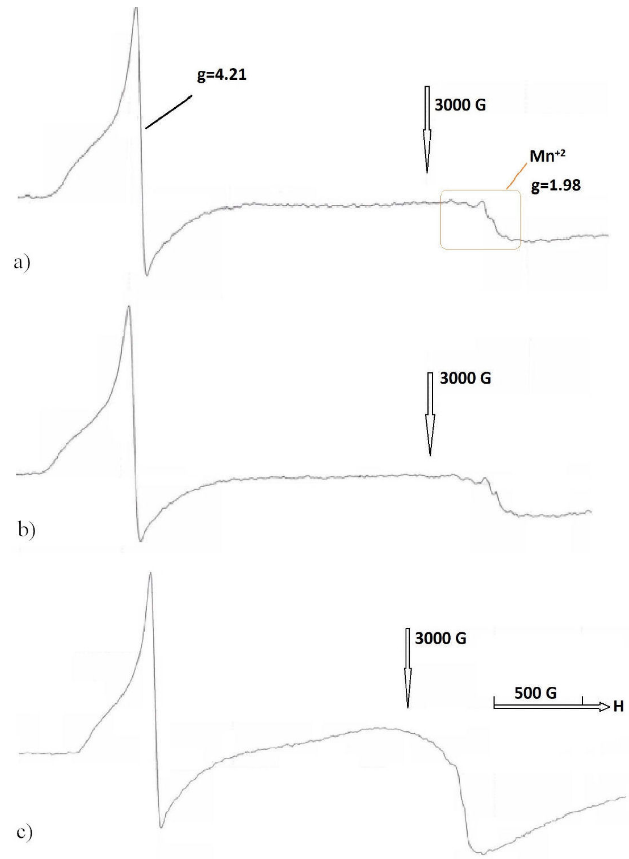

FIGURE 4. EPR spectra of the samples W1 a) W2 b) and W3 c).

3.4. Radiation protection analysis

Phy-X/PSD code was used to calculate radiation attenuation parameters with the chemical compositions (w%) of the samples determined by EDS (Table II). The MAC values changed with incident energies (1 keV-100 GeV) are shown in Fig. 5a). The changes in MAC results are affected by the processes at low (0.001-0.1 MeV), mid (0.1-5 MeV) and high energies (>5 MeV) correspond to photoelectric effect (PE), compton scattering (CS) and pair production (PP), respectively. The LAC values varied with photon energies as seen in Fig. 5b). MAC values and material's density are the factors affect LAC parameter. Additionally, the MAC results of the samples are compared with previously reported ordinary concrete (OC) [32] and cement [33] [Fig. 5c)]. The MAC values and so the shielding efficiencies of the samples can be ordered as W3>W1>W2>Cement>OC. Among the samples, W3 has the highest shielding ability, while W2 has the least. According to the results obtained at all energies, the common feature is that all samples have better protection potential than OC.

The MFP and HVL values changed with photon energies are given in Fig. 6. If the material has higher values of HVL and MFP, it is known as the worst shield. The highest values of HVL and MFP and so the lowest shielding performance is found for W2, whereas the highest one is obtained for W3.

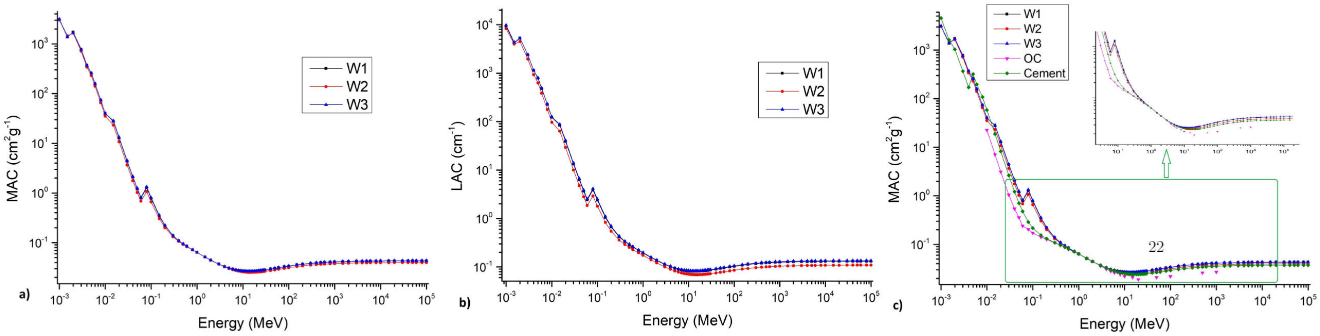

FIGURE 5. The variations of MAC a) LAC b) and the comparison of MAC values with OC and cement c) versus photon energies.

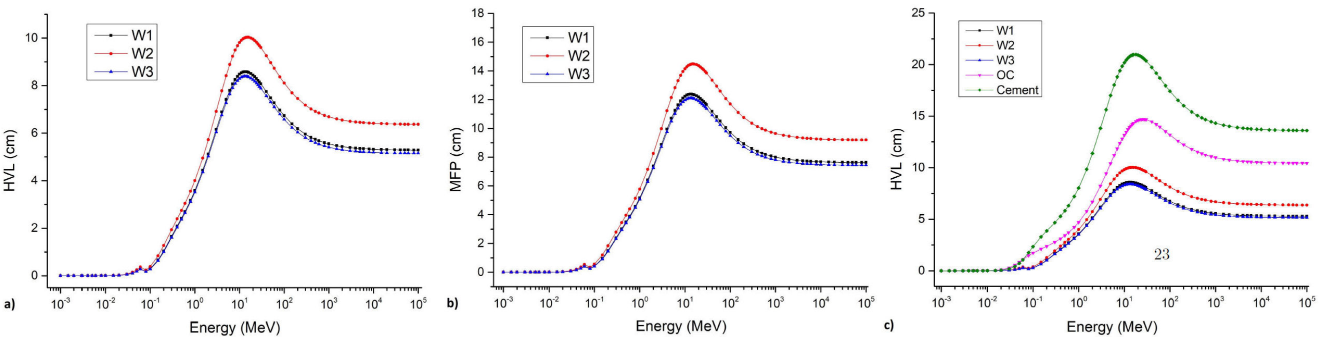

FIGURE 6. The variations of HVL a) MFP b) and the comparison of HVL values with OC and cement c) versus photon energies.

The radiation shielding capability (RSC) of the samples are compared by OC and cement [Fig. 6c)]. It is concluded that the HVL values of the samples are lower than those of OC and cement.

The Z_{eff} values changed with photon energy is demonstrated in Fig. 7. In the low energy region (0.001-0.1 MeV), the PE cross-section (Z^{4-5}); in the mid-energy region (0.1-5 MeV), CS cross-section (E^{-1}) and in the high energy region (>5 MeV), PP cross-section (Z^2) are effective and therefore Z_{eff} values increase, decrease and are stable, respectively. Z_{eff} values can be influenced due to the elements with distinct

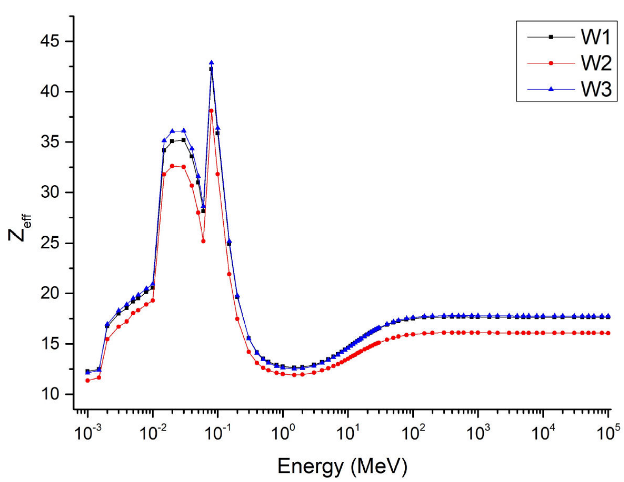

FIGURE 7. The variations of Z_{eff} versus photon energies.

atomic numbers in the material. As, Z_{eff} is the atomic number of a material containing more than one element, structure with large atomic number differences cause fluctuations. The samples with W content have the highest Z_{eff} values and this kind of fluctuations. Thus, W3 has the highest shielding performance depending on Z_{eff} values.

The EBF and EABF varied with photon energies are given in Figs. 8-9. In the low, mid and high energy regions, EBF and EABF are lower, higher and again lower based on the PE, CS and PP effects, respectively. According to the obtained EBF and EABF values, the photons cluster more for W3 among the samples. So, it is seen that W3 shows the CS process is effective.

Attenuation of fast neutron of the samples was also achieved by the code and the cross sections are given as 0.092, 0.085 and 0.094 for W1, W2 and W3, respectively. The highest neutron attenuation is found for W3, the lowest one is for W2 like photon shielding. It can be also concluded that FNRCS values of W3 are better than those of the previously studied OC (0.093).

4. Conclusions

The goal of the study was to develop alternative materials based on reusing of wastes for obtaining higher shielding features. To this end, RSC and spectroscopic details of the waste samples were determined by Phy-X/PSD code and the techniques. EPR spectra of the samples give an EPR signal with

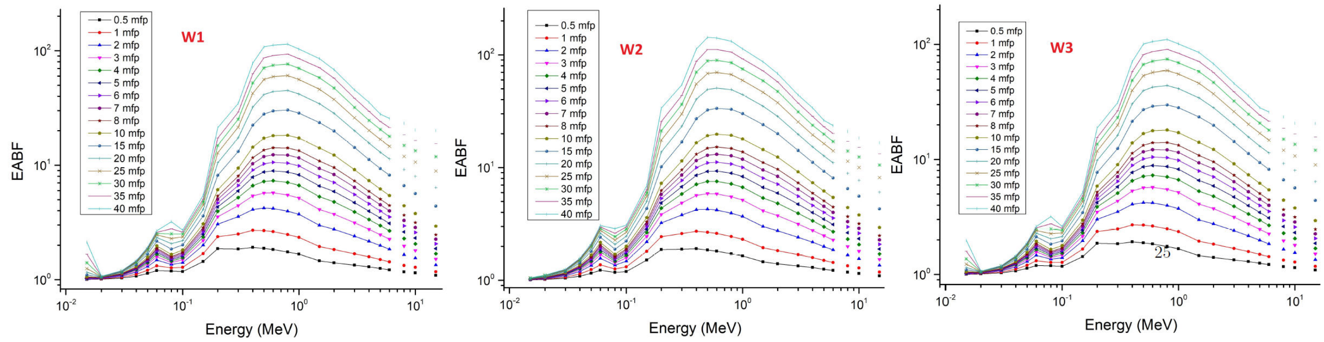

FIGURE 8. The changes of EABF values of the samples versus photon energies.

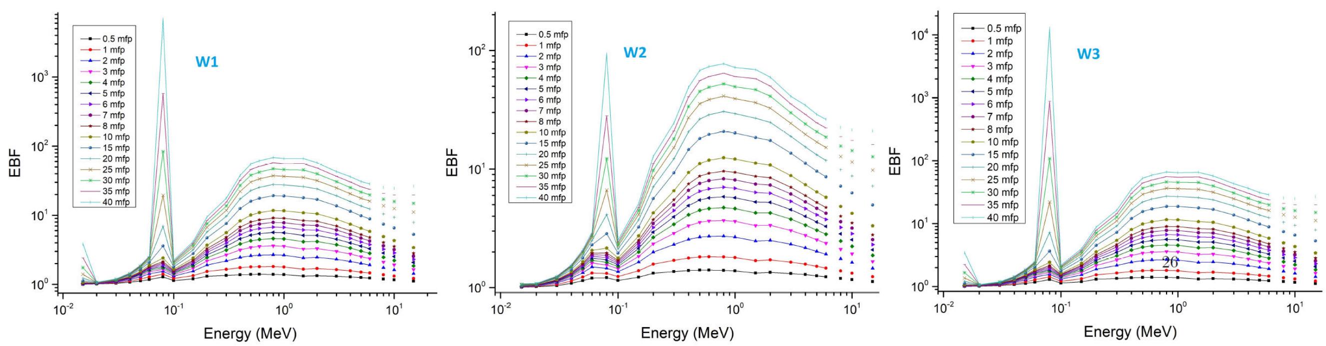

FIGURE 9. The changes of EBF values versus photon energies.

g value of 4.21 which is attributed to ferric center and signal with g value of 1.98 corresponds to Mn^{+2}. The XRD spectra show the amorphous structure with some crystallites. Computational results of radiation attenuation parameters, it would be useful to point out that the existence of heavy metal W content with higher atomic number in the sample improves the protection performance. In addition, it can be noted that the neutron attenuation capacity of W3 is the highest, similar to the photon attenuation property. As a result, all of the designed waste samples based on waste glass can be recommended as new protective materials. With this study, we wanted to show that these types of materials, which are used as ornaments or commercially and whose waste is abandoned in empty lands, can be used more functionally and for different purposes.

Acknowledgement

Experimental results were obtained from Advanced Technology Research & Application Center (ILTEK) of Selcuk University.

Statements and declarations

Competing interests

The authors declare that they have no known competing financial interests or personal relationships that could have appeared to influence the work reported in this paper.

Ethics approval

Not applicable

Consent to participate

Not applicable

Consent for publication

Not applicable

Author contributions

All authors contributed to the study conception and design. Material preparation, data collection and analysis were performed by Zeynep AYGUN and Murat AYGUN. The first draft of the manuscript was written by Zeynep AYGUN and all authors commented on previous versions of the manuscript. All authors read and approved the final manuscript.

Availability of data and materials

Data of this study are available from the corresponding author on responsible request.

Funding

This work was supported by Bitlis Eren University Scientific Research Projects Coordination Unit (BEBAP) with a project grant number 2023.14.

1. M. Aygun, Z. Aygun, and E. Ercan, Radiation protection efficiency of newly produced W-based alloys: Experimental and computational study, *Radiat. Phys. Chem.* **212** (2023) 111147, https://doi.org/10.1016/j.radphyschem.2023.111147
2. T.H. Khazaalah, I.S. Mustafa, and M.I. Sayyed, Radiation parameterizations and optical characterizations for glass shielding composed of SLS waste glass and lead-free materials, *Nucl. Eng. Technol.* **54** (2022) 4708, https://dx.doi.org/10.1016/j.net.2022.08.009
3. M. Elsafi, N. Almousa, N. Al-Harbi, M.N. Almutiri, S. Yasmin, and M.I. Sayyed, Ecofriendly and radiation shielding properties of newly developed epoxy with waste marble and WO3 nanoparticle, *J. Mater. Res. Technol*. **22** (2023) 269, https://dx.doi.org/10.1016/j.jmrt.2022.11.128
4. M.R. Bawani, A.I. Arol, G. Tozsin, and A. Torun, Conversion of cleaned Oltu-stone wastes (a semi-precious stone) into a valuable product using binderless agglomeration, *Physicochem. Probl. Miner. Process.* **59** (2023) 169730, https://doi.org/10.37190/ppmp/169730
5. M. Hatipoglu, D. Ajò, Y. Kibici, and D. Passeri, Natural carbon black (Oltu-stone) from Turkey: a micro-Raman study, *N. Jb. Miner. Abh.* **189/1** (2012) 97, https://doi.org/10.1127/0077-7757/2012/0211
6. S. Toprak, Petrographical properties of a semi-precious coaly stone, Oltu stone, from eastern Turkey, *Inter. J. Coal Geology* **120** (2013) 95, https://doi.org/10.1016/j.coal.2013.10.004
7. N. Ural, and G. Yakşe, Utilization of marble piece wastes as base materials, *Open Geosci.* **12** (2020) 1247, https://doi.org/10.1515/geo-2020-0197
8. C. Ince, S. Derogar, N. Yardımcı Tiryakioglu, and Y.C. Toklu, The influence of zeolite and powdered Bayburt stones on the water transport kinetics and mechanical properties of hydrated lime mortars, *Const. Building Mater.* **98** (2015) 345, https://doi.org/10.1016/j.conbuildmat.2015.08.118
9. K. Günoğlu, and I. Akkurt, Gamma-ray attenuation properties carbide compounds (WC, Mo2C, TiC, SiC, B4C) using Phy-X/PSD software, *IJASRAR* **1** (2023) 1, https://www.ijasrar.com/index.php/ijasrar/article/view/6
10. Z. Aygun, M. Aygun, and N. Yarbasi, A study on radiation shielding potentials of green and red clayey soils in Turkey reinforced with marble dust and waste tire, *J. New Results in Sci.* **10** (2021) 46, https://doi.org/10.54187/jnrs.986038
11. Z. Aygun and M. Aygun, A study on usability of Ahlat ignimbrites and pumice as radiation shielding materials, by using EpiXS code, *Int. J. Environ. Sci. Technol.* **19** (2022) 5675, https://doi.org/10.1007/s13762-021-03530-9
12. Z. Aygun and M. Aygun, Radiation Shielding Potentials of Rene Alloys by Phy-X/PSD Code, *Acta Phys. Polonica A* **5** (2022) 507, https://doi.org/10.12693/APhysPolA.141.507
13. Z. Aygun and M. Aygun, A computational study on radiation shielding performances of self-passivating tungsten alloys, *J. Theor. Appl. Phys.* **17** (2023) 1, https://doi.org/10.57647/J.JTAP.2023.1705.52
14. M. Aygun and Z. Aygun, A comprehensive analysis on radiation shielding characteristics of borogypsum (boron waste) by Phy-X/PSD code, *Rev. Mex. Fis.* **69** (2023) 040401, https://doi.org/10.31349/RevMexFis.69.040401
15. Z. Aygun and M. Aygun, A Theoretical Study on Radiation Shielding Characteristics of Magnetic Shielding Alloys, Ni80Fe15Mo5 and Ni77Fe14Cu5Mo4, by Determining the Photon Attenuation Parameters in the Energy Range of 15keV-100GeV, *Karaelmas Sci. Engineer. J.* **11** (2021) 165, https://doi.org/10.7212/karaelmasfen.900452
16. F. Aliyah, I. Kambali, A.F. Setiawan, Y.Md Radzi and A. Abdul Rahman, Utilization of steel slag from industrial waste for ionizing radiation shielding concrete: A systematic review, *Const. Building Mater.* **382** (2023) 131360, https://doi.org/10.1016/j.conbuildmat.2023.131360
17. G. ALMisned, D. Sen Baykal, E. Ilik, G. Kilic, and H.O. Tekin, The role of ZrO2 as glass-network former on radiation transmission properties of aluminoborosilicate (ABS) glasses: A glass type for nuclear waste immobilization, *Ceramics Inter*. **49** (2023) 39124, https://doi.org/10.1016/j.ceramint.2023.09.252
18. E. Sakar, O.F. Ozpolat, B. Alm, M.I. Sayyed, and M. Kurudirek, Phy-X / PSD: Development of a user-friendly online software for calculation of parameters relevant to radiation shielding and dosimetry, *Radiat. Phys. Chem*. **166** (2020) 108496, https://doi.org/10.1016/j.radphyschem.2019.108496
19. C. Xiang *et al*., Design of single-phase high-entropy alloys composed of low thermal neutron absorption cross-section elements for nuclear power plant application, *Intermetal.* **104** (2019) 143, https://doi.org/10.1016/j.intermet.2018.11.001
20. D.F. Jackson and D.J. Hawkes, X-ray attenuation coefficients of elements and mixtures, *Phys. Reports* **70** (1981) 169, https://doi.org/10.1016/0370-1573(81)90014-4
21. ANSI/ANS 6.4.3, Gamma-ray Attenuation Coefficients and Buildup Factors for Engineering Materials. American Nucl Soc, La Grange Park, Illinois, (1991).
22. Y. Harima, Y. Sakamoto, S. Tanaka, and M. Kawai, Validity of geometric progression formula in approximating gamma-ray buildup factors, *Nucl. Sci. Engineer*. **94** (1986) 24, https://doi.org/10.13182/NSE86-A17113
23. Y. Harima, An historical review and current status of buildup factor calculations and applications, *Radiat. Phys. Chem*. **41** (1993) 631, https://doi.org/10.1016/0969-806X(93)90317-N
24. Z. Aygun, AFM and SEM Studies of VO2+ Doped Potassium Dihydrogen Citrate Single Crystal Obtained by Slow Evaporation Method, *J. Chem. Crystallogr.* **43** (2013) 103, https://doi.org/10.1007/s10870-013-0391-4

25. T. Thriveni, S.Y. Nam, and J.W. Ahn, Enhancement of arsenic removal efficiency from mining waste water by accelerated carbonation. *IMPC* (2014) 1,

26. B. Yu, G. Fan, S. Zhao, Y. Lu, Q. He, Q. Cheng, J. Yan, B. Chai, and G. Song, Simultaneous isolation of cellulose and lignin from wheat straw and catalytic conversion to valuable chemical products. *Appl. Biol. Chem.* **64** (2021) 15, `https://doi.org/10.1186/s13765-020-00579-x`

27. P. Scherrer, Bestimmung der Grösse und der inneren Struktur von Kolloidteilchen mittels Röntgenstrahlen, *Nachr. Ges. Wiss. Göttingen* **26** (1918) 98,

28. Z. Aygun and M. Aygun, Spectroscopic analysis of Ahlat stone (ignimbrite) and pumice formed by volcanic activity, *Spectrochim. Acta A* **166** (2016) 73, `https://doi.org/10.1016/j.saa.2016.05.018`

29. Z. Aygun, M. Aygun, B. Karabulut, and A. Karabulut, Investigation of non-irradiated and gamma-irradiated Trommel Sieve Waste (TSW) with EPR technique, *Annl Nucl. Energy* **40** (2012) 84, `https://doi.org/10.1016/j.anucene.2011.10.015`

30. C.L. Hawkins, and M.J. Davies, Detection and characterisation of radicals in biological materials using EPR methodology, *Biochim. et Biophys. Acta* **1840** (2014) 708, `https://dx.doi.org/10.1016/j.bbagen.2013.03.034`

31. I. Markevich *et al*., The interaction of Mn-related centers with the centers of photosensitivity in doped ZnO materials, J. *Mater. Sci. Mater. Electron* **34** (2023). `https://dx.doi.org/10.1007/s10854-023-10042-4`

32. I.I. Bashter, Calculation of radiation attenuation coefficients for shielding concretes, *Ann. Nucl. Energy* **24** (1997) 1389, `https://doi.org/10.1016/S0306-4549(97)00003-0`

33. N. Sathiparan and H.T.S.M. De Zoysa, The effects of using agricultural waste as partial substitute for sand in cement blocks, *J. Building Engineer*. **19** (2018) 216, `https://doi.org/10.1016/j.jobe.2018.04.023`